JOURNAL OF NEUROPHYSIOLOGY
Vol. 59, No. 3, March 1988. *Printed in U.S.A.*

Developmental Changes in Na^+ Conductances in Rat Neocortical Neurons: Appearance of a Slowly Inactivating Component

JOHN R. HUGUENARD, OWEN P. HAMILL, AND DAVID A. PRINCE

Department of Neurology, Stanford University Medical Center, Stanford, California 94305

SUMMARY AND CONCLUSIONS

1. Na^+ conductances have been characterized in rat neocortical neurons from the sensorimotor area. Neurons were obtained by acute dissociation from animals at developmental stages from embryonic *day 16* (*E16*) to postnatal *day 50* (*P50*) to quantify any developmental changes in the kinetic properties of the Na^+ conductance.

2. Neurons were divided into two classes, based on morphology, to determine whether there are any cell-type specific differences in Na^+ conductances that contribute to the different action potential morphologies seen in current-clamp recordings in vitro.

3. Upon isolation, neurons were voltage clamped using the whole-cell variation of the patch-clamp technology. Both cell types, pyramidal and nonpyramidal, demonstrate large increases in Na^+ current density during this developmental period (*E16–P50*). Normalized conductances were near 10 $pS/\mu m^2$ in neurons from embryonic animals, and increased 6- to 10-fold during the first 2 wk postnatal. The final conductance reached in pyramidal neurons was higher than in nonpyramidal neurons.

4. We found no differences between the two cell types, pyramidal and nonpyramidal, in the voltage dependence of activation, inactivation kinetics, voltage dependence of steady-state inactivation, and recovery from inactivation.

5. The time course of Na^+ current in immature neurons were fit with classical Hodgkin-Huxley kinetics. However, in more mature neurons the kinetics of inactivation became more complicated such that two decay components were required to obtain good fit. The slowly decaying component had a time course 5 to 10 times slower than the fast component.

6. Several procedures were used to reduce the magnitude of Na^+ conductance in mature neurons to ensure graded, voltage-dependent inward currents. These included reduced extracellular [Na^+], submaximal tetrodotoxin concentrations, and reduced holding potential. Under each of these conditions we were able to verify the observation that Na^+ current inactivation occurs with two exponentials.

7. Single-channel Na^+ currents were obtained from cell-attached patches. The membrane density of active Na^+ channels increases with development, and ensemble averages from mature neurons demonstrated two inactivation processes. The slow inactivation process was accounted for by long-latency single-channel openings of the same amplitude as the short-latency openings.

8. We conclude that there are no kinetic differences in the Na^+ channels between cell types. Differences in action potentials are then not explained by differences in Na^+ current kinetics, but might be partially explained by the different densities. The developmental increase in Na^+ current density, which is related to an increase in the number of channels per unit membrane area, underlies the increased rate of rise of action potentials in neurons during maturation. The increase in a slowly inactivating component with development affects near-threshold functions such as the persistent inward current that contributes to repetitive firing.

INTRODUCTION

During development, significant changes occur in both the synaptic potentials and intrinsic membrane properties of mammalian neocortical neurons. For example, immature rat cortical neurons have longer action potential (AP) duration, lower amplitude APs, and a more linear membrane conductance in the membrane potential range near rest (25, 29). Also, there are differences in the excitability of different cell types within the neocortex at the same developmental stage (10, 28). Compared with the interneurons, the principle neurons or pyramidal cells have longer AP duration, less pronounced AP undershoots, and different repetitive firing responses to prolonged current pulses.

Recent advances in the isolation of central neurons (24, 35) as well as the application of the patch clamp (19), which permits the study of such neurons, now allow quantitative biophysical studies of the active and passive conductance mechanisms, which account for the intrinsic properties of neocortical neurons.

We report here the developmental changes in inward Na^+ currents that occur in rat neocortical pyramidal and nonpyramidal neurons. The currents recorded in neurons from immature neocortex are small and can be described by standard Hodgkin-Huxley-type kinetics; there are no apparent cell specific differences at early developmental stages. In contrast, neurons obtained from the cortex of more mature (older than postnatal *day 6, P6*) rats generate larger currents (amplitudes up to 10-fold those in immature neurons) and standard kinetic description of the currents no longer applies. Na^+ currents in mature neurons are more complicated in that inactivation follows two decay processes, fast and slow, compared with the simple fast decay in immature neurons. The slow phase of inactivation would contribute to a relatively persistent inward current. This current is similar to yet more rapidly inactivating than the noninactivating current that has been suggested by current-clamp recordings in pyramidal neurons in the hippocampal (21) and neocortical (10) slice, as well as in voltage-clamp recordings obtained from

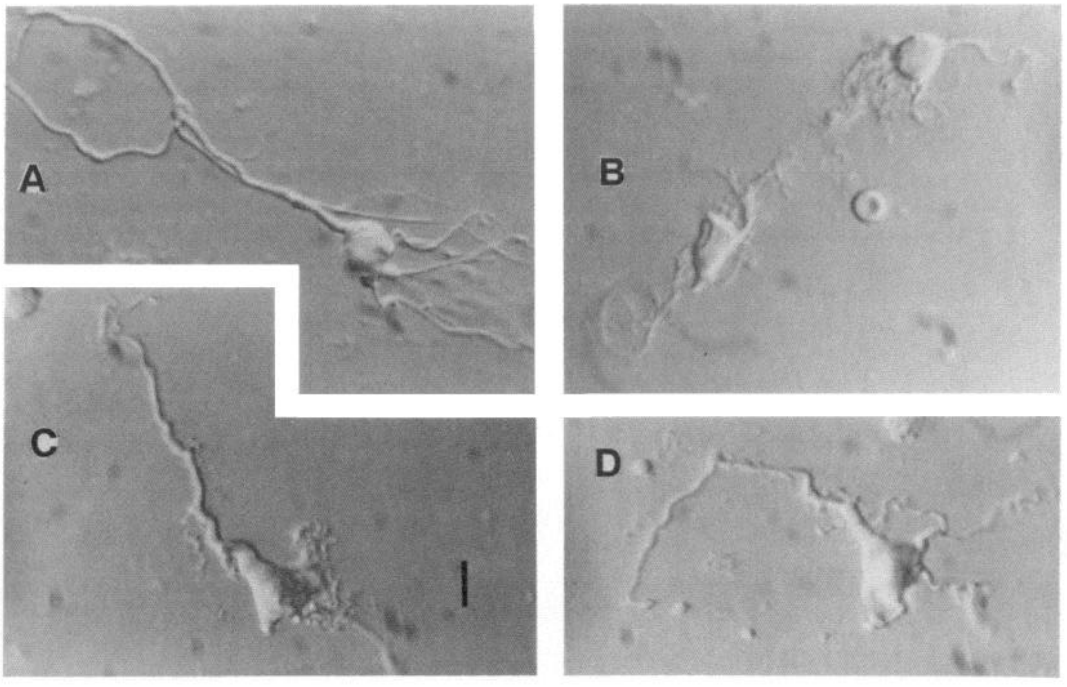

FIG. 1. Morphology of acutely isolated rat *P10* neocortical neurons. Normal dissociation procedures were used (see METHODS.) Cells were viewed and photographed with Hoffman modulation contrast optics. *A, C,* and *D*: individual neurons with pyramidal morphology. *B*: 2 nonpyramidal neurons within the same microscopic field. Scale bar in *C* is 10 μm.

pyramidal neurons in cat sensorimotor cortex (42) and rat hippocampal neurons (15). We also find that nonpyramidal neurons as a group tend to have lower Na^+ channel densities than pyramidal neurons.

With the exception noted above of a relatively higher fraction of slow component in more mature neurons, there were no differences in either the kinetics of activation, inactivation, steady-state inactivation, or recovery from inactivation of peak Na^+ current with either development or between cell types. Part of this work has been published in preliminary form (18, 23).

METHODS

Rat neocortical neurons were obtained by the following procedure, derived from that of Wong and colleagues (24, 35). Pregnant Sprague-Dawley rats (Simonsen Breeders) were housed in the local animal facility. Cells were obtained either from embryos at *E16–E21*, delivered by cesarean section under pentobarbital anesthesia (50 mg/kg), or on postnatal *day 1-30*. Animals were anesthetized by cooling in an ice bath, and then decapitated. The brain was exposed, removed, and several 600-μm-thick coronal slices were cut from the sensorimotor area using a vibratome (Lancer). The pia was gently peeled from each cortical slice with fine forceps, and the underlying (subcortical) white matter cut away with a scalpel blade. Pieces of cortex measuring ~600 microns across were cut from each slice and incubated at 26 ± 0.5°C in a buffered (pH 7.4) saline solution of the following composition (in mM): NaCl 130, KCl 5, $CaCl_2$ 1, $MgCl_2$ 1, *N*-2-hydroxyethylpiperazine-*N'*-2-ethanesulfonic acid (HEPES) 20, dextrose 25, cysteine 0.01; and 1.6 mg/ml papain (type IV, Sigma). The incubation medium was gassed by blowing 95% O_2-5% CO_2 over its surface, and the tissue was gently stirred with a micro stir bar. After 90 min of incubation in the enzyme, the tissue was washed and mechanically dissociated

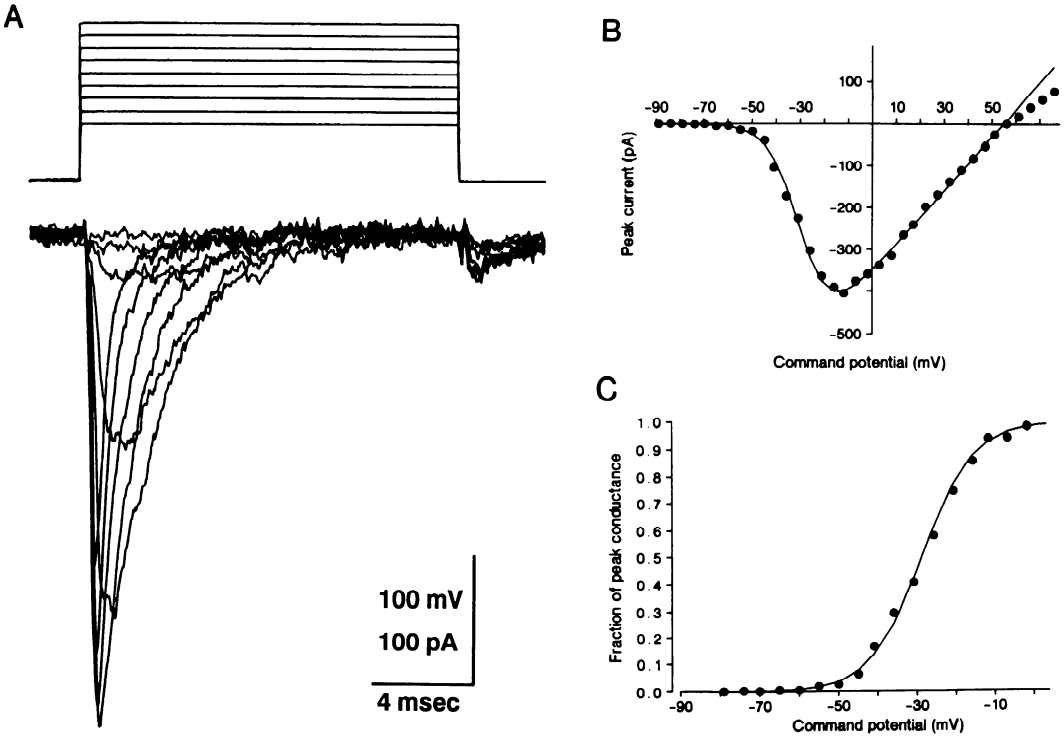

FIG. 2. *A*: whole-cell Na^+ currents recorded from an *E16* pyramidal-shaped neuron. Currents are shown in response to 15-ms step depolarizations starting at −56 mV and incrementing by 10 mV from a holding potential of −100 mV. Leak and capacitive subtraction were applied in this experiment. The upper traces in this and all subsequent figures are the applied voltage commands, and the lower traces are the current responses (downward is inward current). *B*: current-voltage relationship of the peak Na^+ current from *A*. Measured peak current is shown (●); the smooth curve is the best fit according to *Eq. 2*, with $V_{1/2} = -29$ mV, $k = 6.5$ mV per *e*-fold, and $\bar{G}_{Na^+} = 6.4$ nS. *C*: data from *B* plotted as an activation curve for peak current according to *Eq. 2*.

by triturating with polished Pasteur pipettes of decreasing apertures. The tissue suspension was then poured into 35-mm Petri dishes and allowed to settle for 30 min in a gassed holding tank before being transferred to the experimental chamber where superfusion with the bathing medium was begun. When younger animals were used (up to *P14*), the cell yield was normally >500 viable isolated neurons per cortical slice. With more mature animals the cell yield became lower, but viable cells could be obtained for all developmental ages in this study (*E16–P50*). In some cases trypsin (1 mg/ml, type IX, Sigma) was used as the proteolytic agent rather than papain, and no differences in the Na^+ current were observed.

Acutely isolated cortical neurons were viewed with an inverted microscope and Hoffman optics and classified into two general groups based on morphology (see Fig. 1) and immunocytochemistry. Pyramidal type cells had one major apical dendrite that was easily identified, since it was longer and often thicker than the other dendrites.

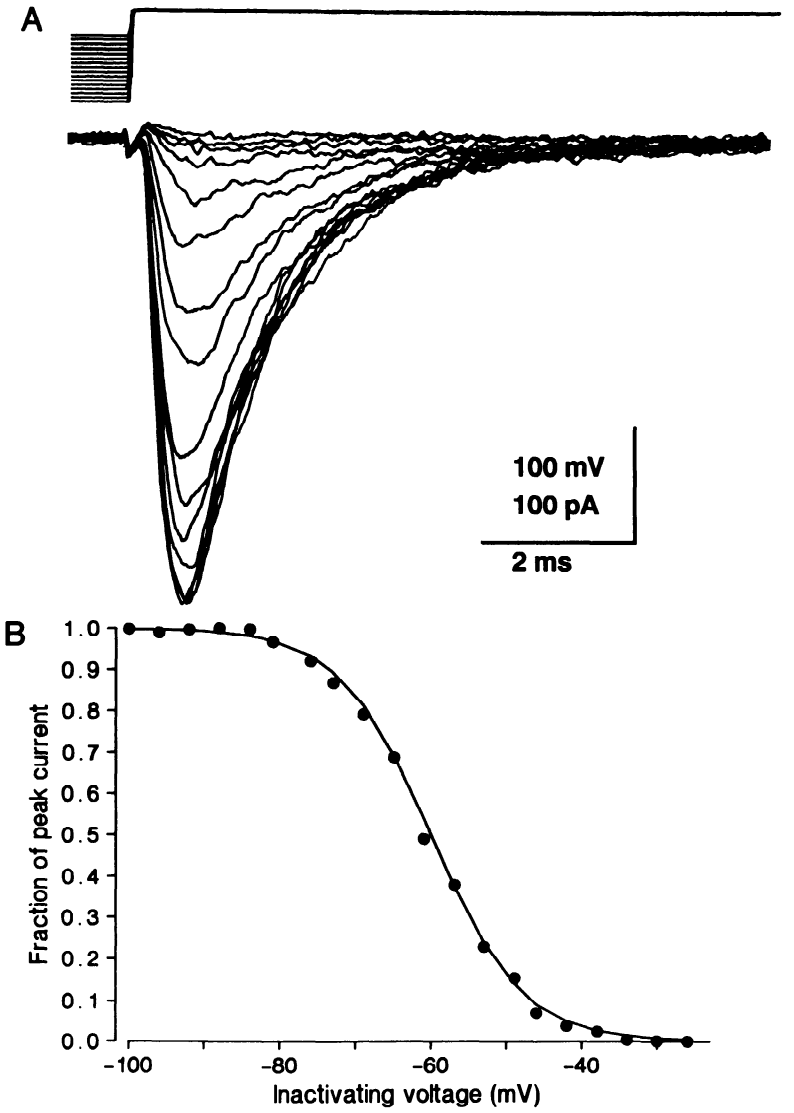

FIG. 3. Steady-state inactivation of Na^+ currents in immature neocortical neurons. *A*: Na^+ currents in an *E18* nonpyramidal neuron under influence of 500-ms inactivating prepotentials. Prepotentials started at −100 mV and were incremented by 3-mV steps while the command potential was kept constant at −10 mV. No leak subtraction applied for this protocol. *B*: the fraction of peak current (h_∞) is plotted vs. the inactivation voltage. The smooth curve is the best fit curve to a Boltzman distribution with values of −60 mV for $V_{1/2}$ and 6.1 mV per *e*-fold for *k*.

It might have several shorter secondary branches. These cells often had triangular-shaped somata from which tufts of basilar dendrites projected. Nonpyramidal neurons (putative interneurons) often had a round soma and were identified by the absence of any one major dendritic process and the presence of bipolar or multipolar processes. These distinctions based on cell morphology were confirmed in experiments where neurons were fixed and processed for immunocytochemistry using an antibody to glutamic acid decarboxylase (GAD) (36) kindly provided by Dr. D. Schmechel. Most cells visually identified as interneurons reacted positively to GAD (the synthetic enzyme for γ-amino butyric acid, GABA) in contrast to the pyramidal neurons, which failed to react. Viable neurons were easily distinguished from nonneuronal elements and unhealthy neurons. Glial cells and fibroblasts were flat in appearance and, when recorded from, demonstrated no active conductances. To further aid in the identification of nonneuronal elements, astrocytes were identified in preliminary experiments using immunocytochemical techniques and an antibody to glial fibrillary acidic protein kindly provided by Dr. L. Eng (39). Unhealthy neurons were swollen, often had large, rounded cell bodies and beaded dendrites, and exhibited very high input (leak) conductance in whole-cell recordings. There was a developmental change in the total membrane area and morphology of individual neurons during the period from *E16* to *P50*. Figure 1 shows examples of dissociated neurons of the two basic morphological cell types from a *P10* animal. Figure 1, *A*, *C*, and *D* shows pyramidal cells, whereas Fig. 1*B* shows nonpyramidal neurons. Younger cells had smaller somata and dendritic processes that were not well developed. Only cells that were clearly identifiable as pyramidal (with a large apical dendrite) or nonpyramidal (with round somata and lack of major dendrites) were used in this study.

Recordings were obtained from isolated neurons using either the cell-attached mode or the whole-cell mode of the patch-clamp technique (19). Electrodes were pulled from thin-walled glass capillaries (W-P Instruments, TW-150), Sylgard (Dow-Corning) coated, and fire polished. A List model EPC-7 (List Instruments) was used as the recording amplifier. Series resistance compensation, to 90% of the estimated patch electrode access resistance, was used during whole-cell experiments. In some cases voltage-clamp recordings were obtained with a high-speed (40 kHz) switching single-electrode voltage clamp (Axoclamp 2A) to record the membrane potential. Data were either recorded on-line into computer memory, (INDEC model 11-73) or stored in pulse-code-modulated form (Neuro-corder, Neuro Data Instruments) on a VHS video tape recorder for later display and analysis.

The superfusion solution contained (in mM) NaCl 145, KCl 3, $MgCl_2$ 1, $CaCl_2$ 1, $CdCl_2$ 0.5,

TABLE 1. *Kinetic properties of Na^+ conductances in rat neocortical neurons at differen. developmental stages*

	Normalized Conductance, pS/μm²	Peak Activation		Steady-State Inactivation		τ Recovery From Inactivation, ms		
						Recovery potential, mV		
		k, mV/e-fold	$V_{1/2}$ mV	k, mV/e-fold	$V_{1/2}$ mV	−120	−100	−80
Immature (*E16–P5*)								
Pyramidal	10.2 ± 2.1 (8)	5.6 ± 0.2	−30.4 ± 2.6 (13)	5.7 ± 0.2	−68.4 ± 3.7 (7)	2.3 ± 0.1 (11)	4.4 ± 0.3 (13)	12.0 ± 1.5 (9)
Nonpyramidal	12.7 ± 3.4 (6)	5.5 ± 0.2	−26.0 ± 1.5 (10)	5.5 ± 0.2	−64.4 ± 2.3 (10)	2.4 ± 0.3 (7)	4.4 ± 0.6 (7)	14.4 ± 1.6 (7)
Young (*P6–P19*)								
Pyramidal	63.0 ± 4.4 (3)	5.4 ± 0.2	−39.4 ± 4.5 (4)	5.9 ± 0.4	−62.6 ± 1.8 (5)	2.2 ± 0.4 (3)	3.7 ± 0.7 (3)	14.1 ± 1.6 (4)
Nonpyramidal	59.6 ± 4.6 (4)	5.4 ± 0.2	−35.2 ± 1.1 (5)	5.6 ± 0.2	−66.4 ± 2.7 (4)	2.3 ± 0.3 (8)	4.8 ± 0.8 (8)	14.2 ± 3.4 (8)
Mature (*P20–P50*)								
Pyramidal	109 ± 39 (9)	5.1 ± 0.2	−30.6 ± 2.8 (16)	6.2 ± 0.2	−65.0 ± 5.5 (3)	1.6 (1)	4.0 (1)	8.0 (1)
Nonpyramidal	58.7 ± 12 (8)	5.4 ± 0.2	−34.1 ± 1.7 (18)	5.9 ± 0.1	−66.2 ± 3.3 (5)			

Values are means ± SE; nos. in parentheses are no. of cells. *k*, voltage-dependent relationship of Na^+ conductance activation; $V_{1/2}$, voltage when Na^+ conductance equals one-half maximum Na^+ conductances. τ, time constant.

and HEPES 10, and was adjusted to pH 7.3 with NaOH. The pipette solution for whole-cell recording consisted of CsF 120, tetraethylammonium Cl 10, NaCl 5, $MgCl_2$ 1, $CaCl_2$ 1, ethylene glycol-bis(β-aminoethyl ether)-*N,N'*-tetraacetic acid (EGTA) 11, and HEPES 10, and was adjusted to pH 7.3 with CsOH. For cell-attached patch recordings the pipette solution consisted of Na aspartate 145, 4-aminopyridine 2, $MgCl_2$ 1, and HEPES 10. Experiments were performed at room temperature (23°C).

With development, as the membrane area and peak Na^+ current became larger, there was a loss of voltage control due to series resistance and space-clamp errors. This loss of control was typified by *1*) a lack of graded inward current responses to voltage steps in the threshold range, which is representative of series resistance errors, and *2*) a delayed onset to peak current; more typical of inadequate space clamp (see Fig. 6*A*). To improve voltage control during activation of Na^+ current in mature neurons, the size of the Na^+

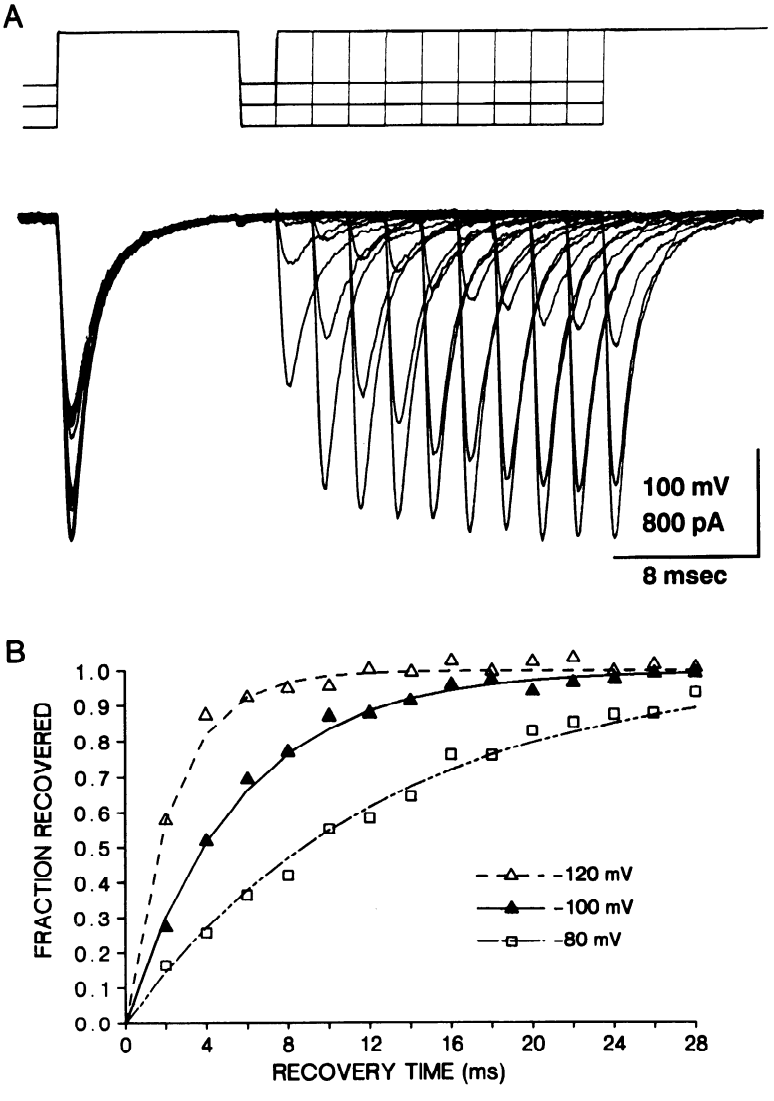

FIG. 4. Time course of recovery from inactivation in immature neurons. *A*: time course of recovery of peak Na^+ current in a *P2* pyramidal neuron at 3 different recovery potentials. Command potential was −30 mV and no leak subtraction was applied. *B*: data from *A* were fit with exponential recovery curves with time constants of 2.3, 5.5, and 12.5 ms at −120, −100, and −80 mV, respectively.

current was reduced by one of the three following methods: *1*) reduced extracellular Na^+ (to 5–16 mM), *2*) reduced holding voltage (−70 to −45 mV), and *3*) the addition of low concentrations (10–100 nM) of tetrodotoxin (TTX) to the superfusion solution. These techniques allowed accurate measurement of the kinetics of Na^+ currents across all developmental ages. However, the estimates of maximum Na^+ conductance (normalized to membrane area, see RESULTS) could not be obtained in these experiments.

Capacitive transients and leak conductance were subtracted by means of a modified P/4 protocol (8), in which the leak currents obtained by scaled hyperpolarizing steps were added to the depolarizing pulses. Current-voltage (*I-V*) curves, activation curves, steady-state inactivation curves, inactivation kinetics, and recovery from inactivation curves were all fit by eye according to the formulas given in RESULTS. The fits are shown in the appropriate figures. Membrane area was estimated from whole-cell capacitance (read from the dial of the EPC-7) assuming a value of 1 $\mu F/cm^2$ (3).

RESULTS

Properties of Na^+ conductances in immature neocortical neurons

The Na^+ currents observed in neocortical neurons obtained from immature rats (younger than *P6*) demonstrate properties consistent with Hodgkin-Huxley type activation (see Fig. 2*A*). The activation of current is voltage dependent, with both the amplitude and kinetics dependent on the command potential. The threshold for activation was around −55 mV, and the peak inward current was obtained near −10 mV. Current-voltage (*I-V*) curves (e.g., Fig. 2*B*) for peak Na^+ current were fit with the following equation

$$I_{\text{peak } Na^+} = (V - V_{Na^+}) \cdot G_{Na^+} \qquad (1)$$

where V is the membrane command potential, V_{Na^+} is the Na^+ equilibrium (Nernst) potential, and G_{Na^+} is the Na^+ conductance de-

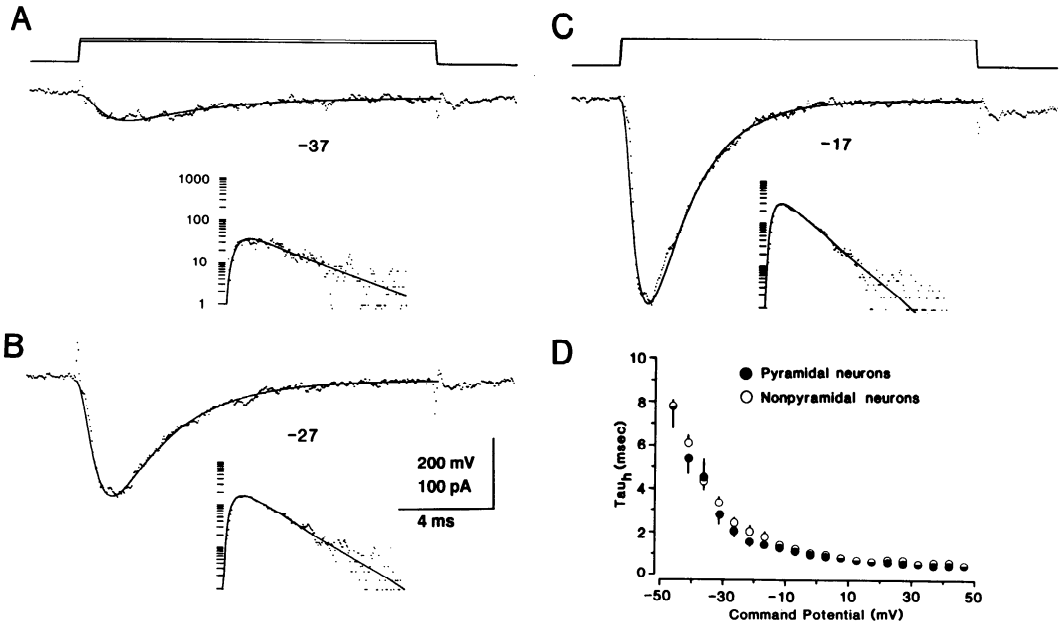

FIG. 5. Time course of Na^+ currents in immature neurons. *A–C*: current traces at 3 potentials are fit to *Eq. 3*. The smooth curves are the best fit, and the data are plotted on semilogarithmic scales in the *inset* of each trace (the semilogarithmic inset in this and all succeeding figures is shown with a time base that is half that in the main figure.) Simple monophasic exponential decay provided an adequate fit for the current recorded at all potentials in this range. Values for τ_h were 4.1, 2.6, and 1.8 ms at command potentials of −37, −27, and −17 mV, whereas the corresponding values of τ_m were 0.70, 0.63, and 0.56 ms. *D*: voltage dependence of τ_h in immature neocortical neurons. These data were obtained from 6 pyramidal neurons and 4 nonpyramidal neurons at *stage P2*, and the error bars represent the standard error of the mean. Where bars are not visible, the error is smaller than the plotted symbol.

rived from *Eq. 2*, below. Alternatively the data from the *I-V* relationship were plotted as activation curves (e.g., Fig. 2*C*). The data points for conductance were obtained by dividing the peak current by the driving force and fit with the following equation

$$G_{Na^+} = \bar{G}_{Na^+}/\{1 + \exp[(V_{1/2} - V)/k]\} \quad (2)$$

where $\bar{G}_{Na^+}$ is the maximum Na^+ conductance at peak current (obtained by linear regression of the slope conductance of the peak *I-V* curve in range of 0 to +40 mV), $V_{1/2}$ is the voltage where G_{Na^+} is one-half of $\bar{G}_{Na^+}$, and k determines the voltage-dependent relationship of G_{Na^+}. In the figure, $\bar{G}_{Na^+}$ is normalized to a value of one.

In neurons from immature neocortex, peak Na^+ currents demonstrate classical steady-state inactivation (Fig. 3*A*). The function of degree of inactivation vs. inactivating voltage was fairly smooth with an *e*-fold reduction per 6 mV. The half-inactivating voltage was around −60 mV (see Fig. 3*B* and Table 1). The time course of recovery from inactivation of peak I_{Na^+} could be reasonably fit with a single exponential and was voltage dependent (Fig. 4*A*), with time constants of ~2, 4, and 10 ms at −80, −100, and −120 mV, respectively (see Fig. 4*B*). This voltage dependency of recovery did not alter with early development or cell type (see Table 1.)

The waveform of the Na^+ current in immature neurons could be fit with standard Hodgkin-Huxley (1952) kinetics using the following equation

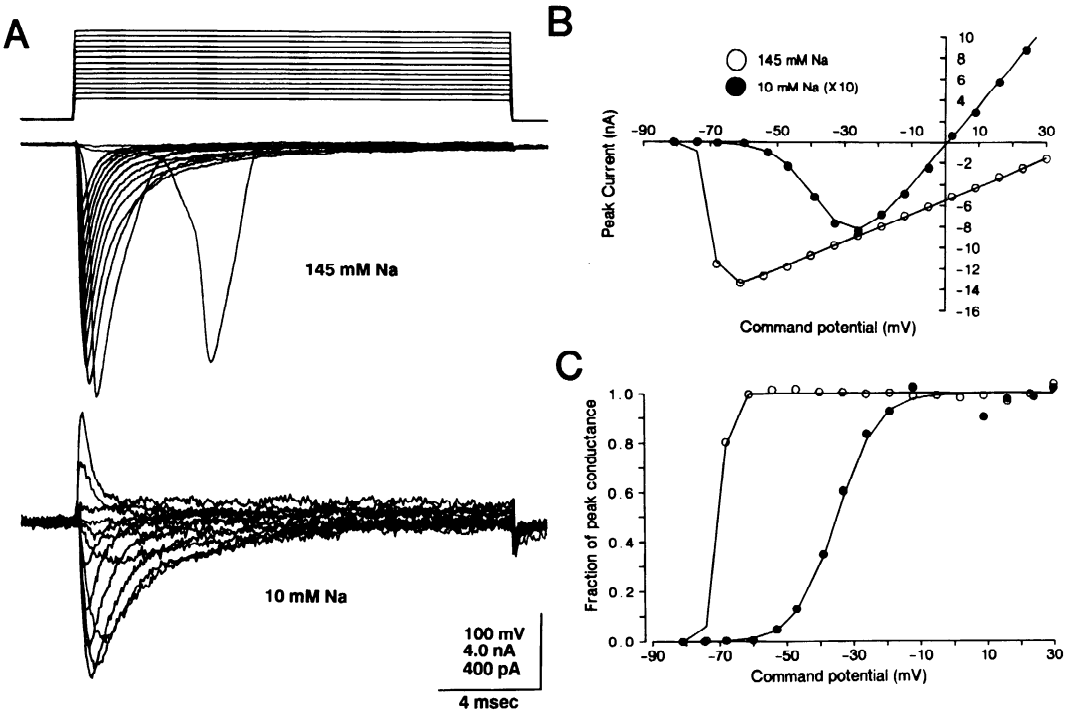

FIG. 6. Loss of voltage control during activation of Na^+ conductance in mature neurons and restoration of control by reducing extracellular $[Na^+]$ ($[Na^+]_o$). *A*: command steps from holding potential of −100 to potentials starting at −73 and incrementing by 7 mV. The upper series of traces is the voltage protocol, the middle traces the Na^+ currents obtained with normal (145 mM) bath [Na], and the lower traces the Na^+ currents obtained with 10 mM bath [Na]. The threshold current in normal $[Na^+]_o$ is quite large (nearly maximal) and with a large delay, whereas in reduced $[Na^+]_o$ the currents increment gradually in amplitude with increasing depolarizations. Note difference in calibration for lowest traces. *B*: current-voltage curves for the 2 situations in *A*. The smooth curves were fit for normal and reduced $[Na^+]_o$ with k values of 6.1 and 1.5 mV per *e*-fold, and $V_{1/2}$ of −35 and −70 mV. Currents in reduced $[Na]_o$ have been scaled up by a factor of 10. *C*: activation curves for data in *A*. In reduced $[Na^+]_o$ the activation is a continuous function of voltage, whereas in normal Na^+ the apparent conductance has gone from 0 to 80% of maximum within 7 mV. Maximum conductance in normal $[Na^+]_o$ was 131 nS, whereas with reduced $[Na^+]_o$ it was 7.0 nS.

$$I_{Na^+} = [1 - \exp(-t/\tau_m)]^3 \times \exp(-t/\tau_h) \cdot G'_{Na^+} \cdot (V - V_{Na^+}) \quad (3)$$

where G'_{Na^+} would be the maximum Na^+ conductance achieved in the absence of inactivation (and corresponds to $\bar{G}_{Na^+} \cdot m_\infty^3 \cdot h_o$, where m_∞ is the final activation reached, and h_o, is the initial inactivation level, see Ref. 20), and τ_m and τ_h are the time constants of activation and inactivation, respectively. The time constants were voltage dependent with both values becoming smaller (faster) with increasing depolarizing commands. Figure 5, *A–C* demonstrates the best Hodgkin-Huxley fit for the Na^+ current at different command potentials from a *E16* neuron. Table 1 presents group data kinetic parameters of Na^+ conductances in neurons from immature and mature neocortex. In immature neurons there were no cell-specific differences in activation, steady-state inactivation, and recovery from inactivation. Figure 5*D* presents the relationship of τ_h vs. membrane potential for the two cell types. In immature neurons, no cell-specific differences were seen.

Properties of Na^+ conductances in mature neocortical neurons

With adequate voltage control, the values for $V_{1/2}$ (−32) and k (6.5 mV per e-fold change in activation) were remarkably constant both with development and between cell types (see Table 1). However the value of $\bar{G}_{Na^+}$, when normalized to membrane area, demonstrated approximately a 10-fold in-

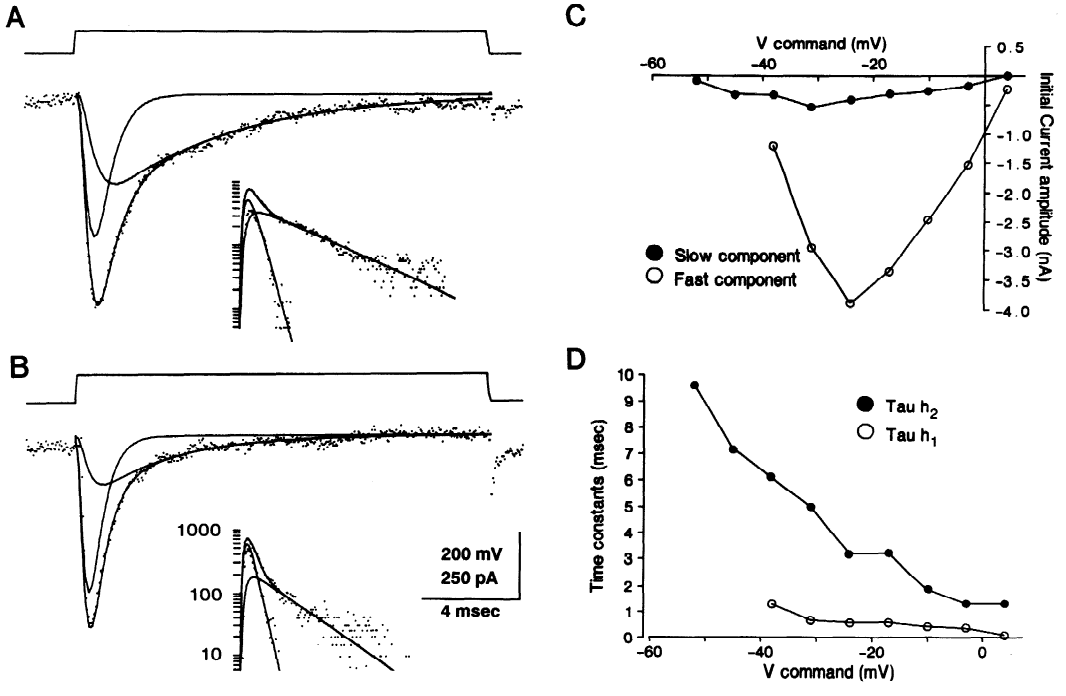

FIG. 7. Kinetic fits to Na^+ currents in mature neocortical neurons. Na^+ currents were reduced in this neuron by using 10 mM extracellular $[Na^+]$ ($[Na^+]_o$). The decay of Na^+ current could not be well fit to a single exponential. *A* and *B*: Hodgkin-Huxley fits (see *Eq. 4*) to currents activated by depolarizations to −32 and −17 mV. The individual components, as well as their sum, are shown as smooth curves in the linear plots and the semilog plots in the *insets*. Kinetic parameters for the fit in *A* were: $\tau_{h1} = 0.62$, $\tau_{h2} = 5.0$, $\tau_m = 0.41$ ms; initial amplitudes were 3.2 nA for the fast component and 0.50 nA for the slow component. The corresponding values in *B* were $\tau_{h1} = 0.51$, $\tau_{h2} = 3.2$, $\tau_m = 0.32$ ms; initial amplitudes were 3.2 nA for the fast component and 0.29 nA for the slow component. *C*: voltage dependence of the amplitude of the 2 components. Initial current amplitude was determined from the zero time intercept of the semilog plots. The slow component has an apparent lower threshold than the fast component. *D*: voltage dependence of the 2 inactivation processes. Both components demonstrate an increase in rate of decay with depolarization.

crease between *E18* and *P30*, from 10 to over 100 pS/μm^2, see Table 1.

With more mature neurons, as the magnitude of the total Na^+ currents increased, there was a loss of voltage control during the depolarizing commands. This was manifest by a sudden voltage threshold for an all-or-none inward current, often a delayed time course of the peak current, and an activation curve that was not well fit by values of $k >$ 2–3 mV per *e*-fold change in activation. In these cases the magnitude of the Na^+ current was experimentally reduced by one of the techniques outlined in METHODS, so that the activation parameters of the Na^+ current could be measured in such cells. Figure 6*A* shows the raw currents and *I-V* curves obtained from one neuron in normal bath solution (145 mM Na^+) and a solution containing 10 mM Na^+. Reduced bath Na^+ re-

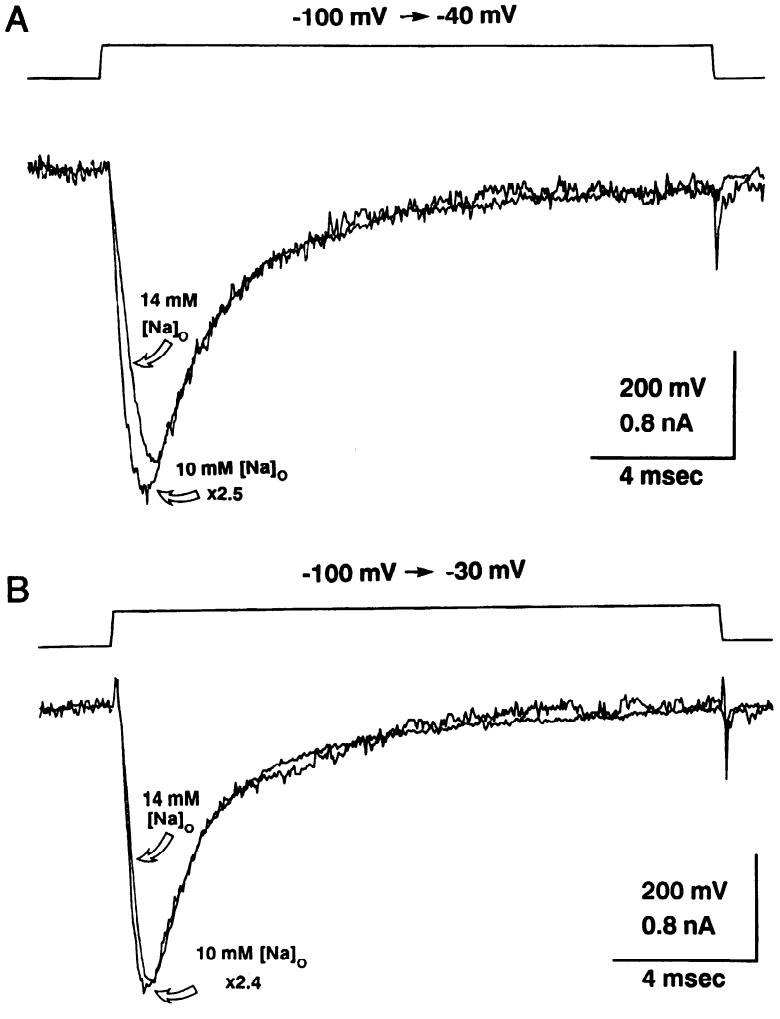

FIG. 8. Under conditions of voltage-clamp control the time course of Na^+ current decay in mature neurons is unaffected by current amplitude. Extracellular [Na^+] ([$Na]_o$) was reduced to 14 mM, and the current-voltage relationship of the peak Na^+ current was determined in a *P17* nonpyramidal neuron. $[Na]_o$ was then further reduced to 10 mM and the protocol repeated. The activation curves for peak Na^+ current under the 2 situations overlapped with identical values for k and $V_{1/2}$ of 6.0 mV per *e*-fold and −34 mV, respectively (not shown). Shown in the figure are scaled currents at 2 sample potentials to demonstrate that the time course of decay is independent of the magnitude of the current and therefore not an artifact of series resistance error.

sulted in smaller Na^+ currents (Fig. 6, *A* and *B*) and a decrease in the slope of activation from 1.5 to 6 mV per *e*-fold (Fig. 6*C*). The numbers in Table 1 for slope and $V_{1/2}$ were tabulated from all neurons with slope >4 under all conditions, including low TTX, reduced extracellular $[Na^+]$ ($[Na^+]_o$), and reduced holding potential. The values for $\bar{G}_{Na^+}$ were only obtained from those few experiments in which normal bath Na^+ was used and the slope was >4 mV per *e*-fold.

With development, the decay component of I_{Na^+} (τ_h) became more complex, and best fit could only be obtained with two components in the following equation

$$I_{Na^+} = I_{Na^+1} + I_{Na^+2} \quad (4)$$

where I_{Na^+1} and I_{Na^+2} are similar to I_{Na^+} in *Eq. 3* with separate values for G'_{Na^+1}, G'_{Na^+2}, τ_{h1}, and τ_{h2}, which are maximum Na^+ conductances and time constants of inactivation of the two components, respectively. Figure 7, *A* and *B* demonstrate the biexponential decay typically obtained from mature neocortical neurons under conditions of voltage clamp. For these fits, separate time constants

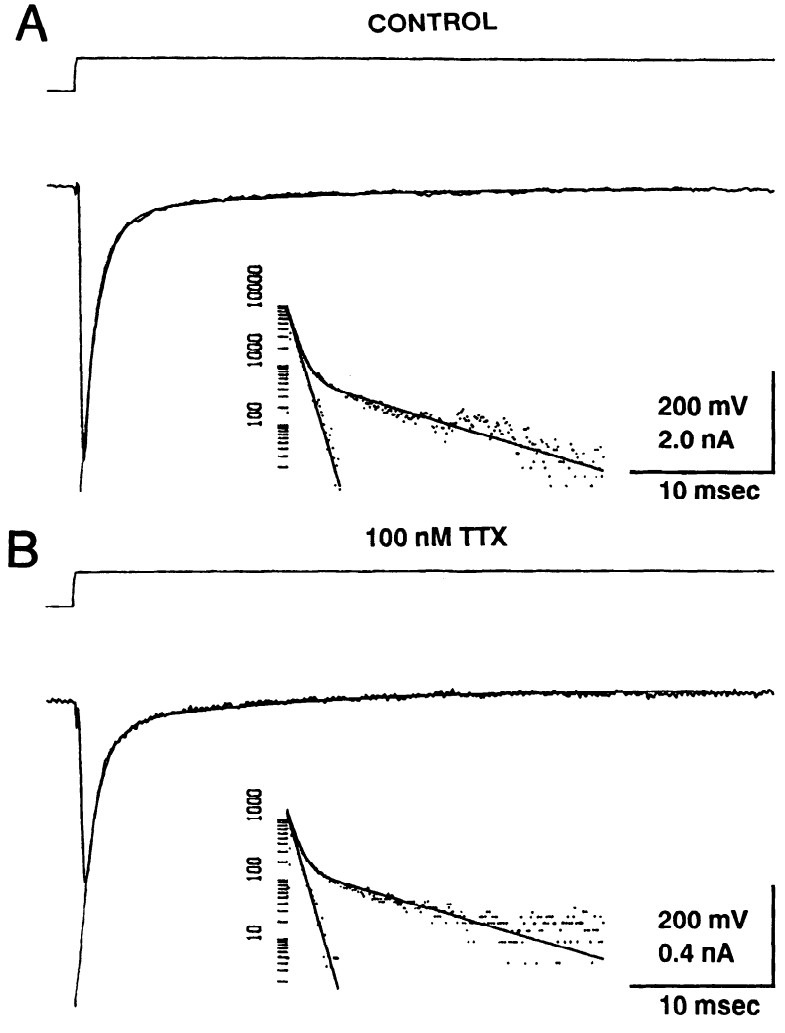

FIG. 9. TTX reduces both components of Na^+ current in mature neurons. *A*: Na^+ currents obtained from a *P14* pyramidal neuron on depolarizing to −40 mV from a holding potential of −100 mV. *B*: with 100 nM TTX added to the bath solution there was an 87% reduction in peak current. As seen in the semilog plots both components were reduced by this concentration of TTX. (Note scale change from *A* to *B*).

of activation for the two components could not be resolved and were assumed to be the same. Both τ_{h1} and τ_{h2} were voltage sensitive in the same manner as τ_h (see Fig. 7*D*). Values for τ_{h1} in mature neurons were similar to the values for τ_h in the embryonic neurons (cf. Figs. 7*D* and 4*B*). Values for τ_{h2} were ~5–10 times larger than τ_{h1}. Also the maximum conductance of the slow component was usually much smaller than that for the fast component (for example, see Fig. 7*C*), but this ratio was variable (range 0.05–0.3) from cell to cell. If the current waveform was dependent on the amount of current (due, for example, to series resistance error), then reducing the amplitude of the series resistance error should alter the shape of the waveform. To test this hypothesis, the amplitude of I_{Na^+} was reduced by either reducing $[Na^+]_o$ or adding submaximal concentrations of TTX to the bath solution. In either case, the result was a reduction in the initial level of each component, with little effect on the kinetics of inactivation. An example of this type of experiment is shown in Fig. 8, where the waveforms of I_{Na^+} under conditions of different $[Na^+]_o$ could be superimposed by scaling the amplitude of the current according to the Nernst driving force. Similar results were obtained in other experiments where 100 nM TTX was added to the extracellular solution to reduce the Na^+ current amplitude. In those situations in which there was no voltage escape under control conditions (e.g., Fig. 9*A*), TTX reduced the amplitude of both components of the inactivation by approximately fivefold without altering the time course of inactivation (Fig. 9*B*). In other experiments, the holding potential was reduced to steady-state inactivate a portion of the total $\bar{G}_{Na^+}$. This resulted in a regaining of voltage control, as determined by a k value of >5 mV per e-fold, yet the two exponential decay components were still evident. (In these cases the ratio of $\bar{G}_{Na^+2}$ to $\bar{G}_{Na^+1}$ was increased due to differential steady-state inactivation; see below.)

In another series of experiments a high-speed switching clamp was used to eliminate series resistance errors, and at the same time monitor the membrane potential during command steps. In four neurons where voltage control was obtained the time course of the Na^+ current was similar to that recorded with normal whole-cell clamp mode using the List EP-7 patch-clamp amplifier when measured currents were <2 nA in peak.

In addition to the differences in rate of inactivation of the two components, other kinetic contrasts were evident, including differential steady-state inactivation and recovery from inactivation of the fast decaying vs. the slow decaying component (not shown). Compared with the rapidly inactivating component (measured as the peak current), the slower component (measured as the residual current amplitude at a latency of 10 ms) inactivated at more depolarized potentials, the voltage dependence of inactivation was less steep (up to 10 mV per e-fold), and the recovery from inactivation was more rapid. There was however, neither a developmental change nor a cell-specific difference in the voltage dependence of steady-state inactivation or recovery from inactivation of the peak current (see Table 1).

The developmental changes in the ratio of slow to fast Na^+ currents are presented in Table 2. Within both the nonpyramidal and pyramidal cell groups there were significant developmental increases in the proportion of slow component to fast component. Linear regression analysis of the same data as in Table 2 demonstrated that the conductance ratio was significantly correlated with age. For nonpyramidal neurons $r = 0.62$, $n = 18$, $P < 0.01$, and for pyramidal neurons $r = 0.59$, $n = 28$, $P < 0.01$.

TABLE 2. *Ratio of slow to fast Na^+ current components in rat neocortical neurons at different developmental stages*

Age	Nonpyramidal Cells	Pyramidal Cells
Immature (younger than *P6*)	0.11 ± 0.030 (7)	0.084 ± 0.013 (15)
Mature (*P6* or older)	0.25 ± 0.051* (11)	0.19 ± 0.030† (13)

Values are means ± SE; nos. in parentheses are no. of cells. Values were obtained fitting the inactivation of sodium currents to a biexponential decay process. Peak extrapolated initial current amplitudes of the slow and fast components were divided to obtain the ratio. * $P < 0.05$ compared with immature nonpyramidal cells; two-tailed t test, $t = 2.50$, df = 16. † $P < 0.01$ compared with immature pyramidal neurons; $t = 3.37$, df = 17.

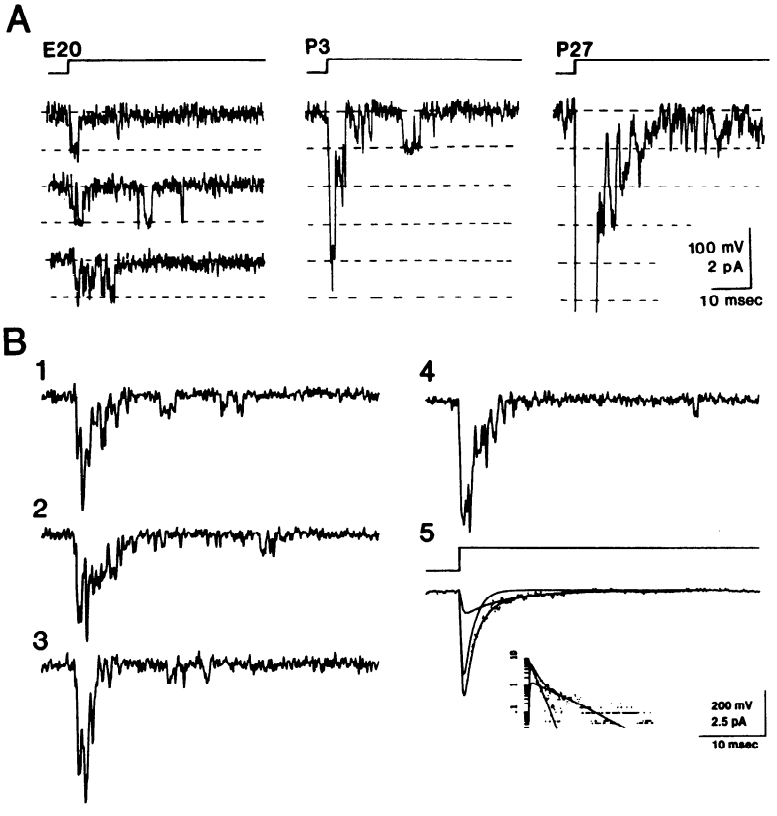

FIG. 10. Single-channel records obtained from cell-attached patches in pyramidal neurons of different developmental stages. *A*: there was an increase in the number of channels that were obtained per each membrane patch (all patches electrodes were of similar size). The stimulus in each case was a 100-mV depolarization to near −30 mV. In the *E20* neuron only single-channel openings were obtained, whereas in the *P3* and *P27* neurons several concurrent openings were observed within the first 10–15 ms followed by late individual openings. In the *P27* neuron the initial current was larger than 15 pA. *B*: single-channel Na^+ currents obtained from a cell-attached patch in a *P10* neocortical neuron. *Traces 1–4* are examples of single sweeps obtained with 100-mV depolarizations to −40 mV. Single-channel openings are seen throughout the duration of these 50-ms depolarizations. *Trace 5* in the lower right is the ensemble average of 50 single sweeps. The best fit for the exponential decay of the ensemble current was obtained with 2 components. Kinetic parameters for the fit were $\tau_{h1} = 1.5$, $\tau_{h2} = 7.4$, $\tau_m = 0.24$ ms; initial amplitudes were 8.9 pA for the fast component and 1.5 pA for the slow component. The fits (both individual components as well as the sum) are shown as solid lines overlaid on the data (discontinuous points) in the linear plot, as well as the semilog plot shown (*inset*).

Properties of single Na^+ channels in neocortical neurons

The increase in Na^+ conductance density could be explained by either an increased current through individual channels or an increased density of channels in the membrane. Recordings from channels in cell-attached patches indicate that the latter explanation is the case. Patch recordings were obtained from 20 neurons between developmental stages *E20* and *P27*. With development there was an increase in the number of single channels per cell-attached patch. Figure 10*A* shows that at embryonic stages only single-channel openings were obtained, but that at progressively older stages there is an increase in the number of concurrent openings, indicating more channels per membrane patch. Also, single-channel current amplitude was the same across this developmental sequence (Fig. 10*A*).

The biexponential nature of Na^+ current decay in mature neurons was verified by recording single-channel Na^+ currents from

cell-attached patches. Examples of single-channel currents from a *P10* neuron are shown in Fig. 10*B*. Single-step depolarizations resulted in a barrage of early channel openings, as well as late individual events with latencies of up to tens of milliseconds. Occasionally bursts of openings were seen that lasted the duration of the depolarization. Ensemble averages of Na^+ channel currents demonstrated two decay components, with similar time constants to those obtained with whole-cell clamp currents (Fig. 10*B*). No significant differences in the amplitudes of the early and late single-channel openings could be detected.

DISCUSSION

Na^+ conductances in isolated neocortical neurons have a number of features similar to those of other excitable membranes that fit the Hodgkin-Huxley model. The peak conductance undergoes steady-state inactivation with a half-inactivated membrane potential near −60 mV. This indicates that, at rest (with a membrane potential around −70 mV), a large fraction of Na^+ channels are not available for activation, and that more channels become available during hyperpolarizations. The consequence of this would be a larger safety factor for AP generation when the membrane is under hyperpolarizing influences such as late inhibitory postsynaptic potentials (31, 32) and slow spike afterhyperpolarizations (22, 28). The current is half-activated at a membrane potential near −30 mV, but the threshold for Na^+ current activation is in the range of −50 to −60 mV, a value that compares favorably with the AP threshold obtained in current-clamp recordings from neurons of the in vitro cortical slice (−50 mV, Ref. 10).

Recently, it has been possible to prepare cloned cDNA from mRNA for Na^+ channel proteins from rat brain (33). Functional channels can then be produced by injecting the mRNA obtained from the cloned cDNA into *Xenopus* oocytes (34). The kinetic properties of these channels have been characterized and are fairly consistent with the results presented here (43). Activation, which was determined by using m_∞, was best fit with half-activation around −41 mV, with a slope of 8.7 mV. In our study we have used peak Na^+ conductance (which more closely corresponds to m_∞^3) for the activation curves. When we determine activation by fitting to m_∞ we find comparable values of −42 mV for half-activation and a slope of 9 mV. Steady-state inactivation in oocytes was fit with values of $V_{1/2} = -64$ mV and $k = 10$ mV. The voltage of half-inactivation was comparable with our results (−62 to −68 mV) but the slope was larger than our value of 6 mV. Although the properties of Na^+ conductance in oocytes are similar in many ways to those recorded in our experiments, there is a significant difference in that the Na^+ channels expressed in oocytes showed only simple (monoexponential) inactivation.

The ontogenetic changes in Na^+ current described here are similar to those seen in insect central nervous system (17), and in avian (4, 5, 30) and murine (26) neurons in culture. The changes in current amplitude in each case can be accounted for by an increase in the density of functional Na^+ channels in the neuronal membrane. The increase in Na^+ channel density correlates with increased rate of rise seen in current-clamp recordings from rat neocortical slices at different developmental stages (25). McCormick and Prince (29) have shown that there is a 10-fold increase in the maximal rate of rise during the upstroke of the TTX-sensitive AP between early postnatal ages and 2–3 wk postnatal in pyramidal neurons of rat neocortical slices, a value that is in good agreement with the results of the current study.

In our experiments there were no cell-specific differences observed in activation, inactivation, recovery from inactivation, and steady-state inactivation for peak current during development of pyramidal and nonpyramidal neurons (Table 1.) Although differences in spike duration between pyramidal and nonpyramidal cells (28) are probably not accounted for by differences in the voltage dependence of the Na^+ channels, they could be due in part to the lower density of Na^+ channels in nonpyramidal neurons. This is because spike duration and height are partially determined by the ratio of K^+ to Na^+ conductance; with all other factors being equal, a high ratio would result in a more rapid repolarization with both shorter amplitude and duration APs. There might be subtle differences between cell types in ratios

of the two Na^+ current components, leading to differences in voltage behavior in the threshold range that could influence repetitive firing. Although nonpyramidal neurons, which are capable of firing repetitively at high frequencies (10, 28), tended to have a larger slow component than the pyramidal neurons, the ratio of the two decay components was quite variable between cells, and the difference between cell types was not significant.

There appears to be a larger component of persistent Na^+ current in older animals (Table 2 and see also Refs. 25, 29). Interestingly, there is a change in the ratio of Na^+ channel-specific toxin binding with development (6). The ratio of saxitoxin to scorpion toxin binding sites increases approximately fourfold from the 1st wk postnatal to adulthood in the rat brain. This change in the binding site ratio may underlie the change in kinetic inactivation, which we have reported here. It has been hypothesized that slowly inactivating or noninactivating current is significant in regulating repetitive firing (21, 41). Because the slowly inactivating current is less sensitive to steady-state inactivation, and recovery from inactivation is faster, this current will be available to help bring the neuron to threshold for a single AP during a prolonged stimulation. In contrast to the slowly inactivating or noninactivating current recorded in in vitro brain slices (15, 21, 41, 42) we do not find evidence of noninactivating current in whole-cell recordings of isolated neocortical neurons. It is possible that either the dissociation procedure or the intracellular perfusion has modified the function of the noninactivating current. However, in cell-attached patches, single-channel openings occurred with latencies as much as tens of milliseconds from the onset of depolarization, and the time constant of decay of whole-cell current slow component was in the range of 5–20 ms. This current would then be important in regulating interspike voltage trajectory when the spike frequency is >50–100 Hz. Nevertheless, the relatively persistent Na^+ current described here is probably only one of several involved in regulation of repetitive firing in neocortical neurons (e.g., Refs. 1, 27). For example, despite the large differences in spike parameters and subthreshold conductances between immature and mature pyramidal neurons, there are not marked differences in the firing behavior (29).

The existence of the a slowly inactivating component of Na^+ current in mature neurons was verified by several procedures that reduced the size of the current and therefore minimized the series resistance error. In addition, single-channel recordings (cell-attached patch) support the whole-cell conclusions: *1*) the number of active Na^+ channels per equivalent patch increases as the neuron matures, and the whole-cell current increases, and *2*) in mature neurons there are two phases of channel activity during a step depolarization: an initial rapid activation and inactivation with many simultaneous openings leading to a large initial peak current, and then brief openings throughout the duration of a depolarization, which correspond to the slowly inactivating current obtained with the whole-cell current recording. Therefore, the mechanism of Na^+ current inactivation in neocortical neurons is quite similar to that demonstrated in neuroblastoma cells (2), i.e., the apparent inactivation of whole-cell Na^+ current is a result of delayed brief openings rather than delayed single-channel inactivation. In contrast to neuroblastoma cells, there is a slower second phase of inactivation in neocortical neurons that can be explained by the very long latency (tens of milliseconds) brief openings (Fig. 10.)

Nonexponential decay of Na^+ is not a unique finding in excitable cells. It has been demonstrated in skeletal muscle in frog (38) and rat (45), in rat heart (37), and frog node (7). However, in contrast to rat neocortex (see Fig. 9), in two of these preparations [rat muscle (37) and frog node (7)] there is a differential TTX sensitivity of the two components. Our results contrast with this finding and are consistent with current-clamp recordings (29) in that we find no difference in TTX sensitivity for Na^+-dependent processes between immature and mature neurons (e.g., Fig. 9.) In support of this conclusion is the finding that the affinity for TTX binding is high from the earliest stages in mouse (13). Thus the two components of inactivation seen in rat neocortical neurons are different from those in rat skeletal muscle and frog node, suggesting that either different

regulation or different types of channels may underlie the slow decay phase in different excitable membranes.

The use of a new method, such as the acute cell dissociation technique employed here, raises a number of questions. For example, there is the possibility that these data are affected by the dissociation procedures (enzymatic and mechanical) and recording conditions such as temperature and the composition of intracellular perfusates. The specific effects of the proteolytic agent papain have been controlled for by using an alternate enzyme (trypsin) in some experiments. No differences in the currents were apparent under these conditions; however, subtle effects due to proteolytic enzymes might have been overlooked. For example, papain is known to block fast inactivation of Na^+ currents (16, 40). However, it is unlikely that this would have affected our results, since the intracellular surface of the membrane must be exposed to the enzyme to affect Na^+ current inactivation. The reduced (23°C) temperature used in these experiments would have effects on Na^+ current amplitude, which can be predicted from the following analysis. McCormick et al. (28) have characterized APs in rat neocortical neurons of the in vitro slice where the maximum rate of rise of APs was in the range of 330–403 V/s at 37°C. When adjusted to room temperature according to the temperature dependence determined by Thompson et al. (Ref. 44, Q_{10} = 1.49) for the maximum rate of rise of APs in hippocampal neurons, values of 190–230 V/s would be expected. The capacitative current required to produce such a change would be ~0.2 nA/pF. The peak currents recorded from acutely isolated cells at −10 mV were in the range 0.3–0.5 nA/pF, values clearly sufficient to produce the expected dV/dt.

Another concern might be generalization of these conclusions to intact neurons. Is the membrane that is responsible for AP generation in vivo maintained after isolation? Perhaps the axon initial segment (9, 11, 12, 46) and hillock, which have a high density of Na^+ channels and contribute to AP generation, do not survive with the soma during the process of dissociation. The above-mentioned similarity in the maximum dV/dt predicted from these results and those from neurons in the slice indicates that the currents recorded in isolation are not grossly different from those present in the more intact in vitro slice preparation. Thus although these questions cannot be completely resolved, the results to date are consistent with what is known from current-clamp recordings from such preparations as the in vitro brain slice (25, 29).

In conclusion, we have begun to identify the specific voltage-dependent conductances that determine the behavior of specific types of individual neurons of in neocortex. This technique presents a promising new approach toward increasing our understanding of the computational properties of the individual units within the cortex.

ACKNOWLEDGMENTS

We gratefully acknowledge the technical support of E. Enayati, J. Kadis, and H. Feeser. C. Joo provided secretarial assistance. We thank R. K. S. Wong and A. Kay for introducing us to the cell dissociation technique and for helpful discussions.

This work is supported by National Institute of Neurological and Communicative Disorders and Stroke Grants NS-06477 and NS-12151, and by the Morris and Pimley Research Funds.

Current address of O. P. Hamill: Dept. of Neurobiology and Behavior, Seeley G. Mudd Hall, Cornell University, Ithaca, NY 14853.

Received 7 July 1987; accepted in final form 30 September 1987.

REFERENCES

1. ADAMS, P. R. AND GALVAN, M. Voltage-dependent currents of vertebrate neurons and their role in membrane excitability. *Adv. Neurol.* 44: 137–170, 1984.
2. ALDRICH, R. W., COREY, D. P., AND STEVENS, C. F. A reinterpretation of mammalian sodium channel gating based on single channel recording. *Nature Lond.* 306: 436–441, 1983.
3. ALMERS, W. Gating currents and charge movement in excitable membranes. *Rev. Physiol. Biochem. Pharmacol.* 82: 96–190, 1978.
4. BADER, C. R., BERTRAND, D., DUPIN, E., AND KATO, A. C. Development of electrical membrane properties in cultured avian neural crest. *Nature Lond.* 305: 808–810, 1983.
5. BADER, C. R., BERTRAND, D., AND KATO, A. C. Membrane currents in a developing parasympathetic ganglion. *Dev. Biol.* 98: 515–519, 1983.

6. BAUMGOLD, J. Changes in the ratio of two separate toxin binding sites on the sodium channel protein during rat brain development. *Brain Res.* 349: 271–274, 1985.
7. BENOIT, E., CORBIER, A., AND DUBOIS, J. Evidence for two transient sodium currents in the frog node of ranvier. *J. Physiol. Lond.* 361: 339–360, 1985.
8. BEZANILLA, F. AND ARMSTRONG, C. M. Inactivation of the sodium channel. I. Sodium current experiments. *J. Gen. Physiol.* 70: 549–566, 1977.
9. CATTERALL, W. A. Localization of sodium channels in cultured neural cells. *J. Neurosci.* 1: 777–783, 1981.
10. CONNORS, B. W., GUTNICK, M. J., AND PRINCE, D. A. Electrophysiological properties of neocortical neurons in vitro. *J. Neurophysiol.* 48: 1302–1320, 1982.
11. COOMBS, J. S., CURTIS, D. R., AND ECCLES, J. C. The interpretation of spike potentials of motoneurones. *J. Physiol. Lond.* 139: 198–231, 1957.
12. COOMBS, J. S., ECCLES, J. C., AND FATT, P. The electrical properties of the motoneurone membrane. *J. Physiol. Lond.* 130: 291–325, 1955.
13. COURAUD, F., MARTIN-MOUTOT, N., KOULAKOFF, A., AND BERWALD-NETTER, Y. Neurotoxin-sensitive sodium channels in neurons developing *in vivo* and *in vitro*. *J. Neurosci.* 6: 192–198, 1986.
14. DICHTER, M. A. Rat cortical neurons in cell culture: culture methods, cell morphology, electrophysiology, and synapse formation. *Brain Res.* 149: 279–293, 1979.
15. FRENCH, C. R. AND GAGE, P. W. A threshold sodium current in pyramidal cells in rat hippocampus. *Neurosci. Lett.* 56: 289–293, 1985.
16. GONOI, T. AND HILLE, B. Gating of Na channels. Inactivation modifiers discriminate among models. *J. Gen. Physiol.* 89: 253–274, 1987.
17. GOODMAN, C. S. AND SPITZER, N. C. The development of electrical properties of identified neurones in grasshopper embryos. *J. Physiol. Lond.* 313: 385–403, 1981.
18. HAMILL, O. P., HUGUENARD, J. R., ENAYATI, E. F., AND PRINCE, D. A. Single channel currents underlying slow threshold Na^+ conductances in rat neocortical neurons. *Soc. Neurosci. Abstr.* 12: 950, 1986.
19. HAMILL, O. P., MARTY, A., NEHER, E., SAKMANN, B., AND SIGWORTH, F. J. Improved patch-clamp techniques for high-resolution current recording from cells and cell-free membrane patches. *Pfluegers Arch.* 391: 85–100, 1981.
20. HODGKIN, A. L. AND HUXLEY, A. F. A quantitative description of membrane current and its application to conduction and excitation in nerve. *J. Physiol. Lond.* 117: 500–544, 1952.
21. HOTSON, J. R. AND PRINCE, D. A. A calcium-activated hyperpolarization follows repetitive firing in hippocampal neurons. *J. Neurophysiol.* 43: 409–419, 1980.
22. HOTSON, J. R., PRINCE, D. A., AND SCHWARTZKROIN, P. A. Anomalous inward rectification in hippocampal neurons. *J. Neurophysiol.* 42: 889–895, 1979.
23. HUGUENARD, J. R., HAMILL, O. P., ENAYATI, E. F., AND PRINCE, D. A. Development of Na^+ conductance in neocortical neurons of the rat. *Soc. Neurosci. Abstr.* 12: 950, 1986.
24. KAY, A. R. AND WONG, R. K. S. Isolation of neurons suitable for patch-clamping from adult mammalian central nervous systems. *J. Neurosci. Methods* 16: 227–238, 1986.
25. KRIEGSTEIN, A. R., SUPPES, T., AND PRINCE, D. A. Cellular and synaptic physiology and epileptogenesis of developing rat neocortical neurons *in vitro*. *Dev. Brain Res.* 431: 161–171, 1987.
26. MACDERMOTT, A. AND WESTBROOK, G. Early development of voltage-dependent sodium currents in cultured mouse spinal cord neurons. *Dev. Biol.* 113: 317–326, 1986.
27. MADISON, D. V. AND NICOLL, R. A. Control of the repetitive discharge of rat CA1 pyramidal neurones *in vitro*. *J. Physiol. Lond.* 354: 319–331, 1984.
28. MCCORMICK, D. A., CONNORS, B. W., LIGHTHALL, J. W., AND PRINCE, D. A. Comparative electrophysiology of pyramidal and sparsely spiny stellate neurons of the neocortex. *J. Neurophysiol.* 54: 782–806, 1985.
29. MCCORMICK, D. A. AND PRINCE, D. A. Post-natal development of electrophysiological properties of rat cerebral cortical pyramidal neurones. *J. Physiol. Lond.* 393: 743–762, 1987.
30. MORI-OKAMOTO, J., ASHIDA, H., MARU, E., AND TATSUNO, J. The development of explanted cortical neurons from chick embryos. *Dev. Biol.* 97: 408–416, 1983.
31. NEWBERRY, N. R. AND NICOLL, R. A. A bicuculline-resistant inhibitory post-synaptic potential in rat hippocampal pyramidal cells *in vitro*. *J. Physiol. Lond.* 348: 239–254, 1984.
32. NICOLL, R. A. AND ALGER, B. E. Synaptic excitation may activate a calcium-dependent potassium conductance in hippocampal pyramidal cells. *Science Wash. DC* 212: 957–959, 1981.
33. NODA, M., IKEDA, T., KAYANO, T., SUZUKI, H., TAKESHIMA, H., KURASAKI, M., TAKAHASHI, H., AND NUMA, S. Existence of distinct sodium channel messenger RNAs in rat brain. *Nature Lond.* 320: 188–192, 1986.
34. NODA, M., IKEDA, T., SUZUKI, H., TAKESHIMA, H., TAKAHASHI, T., KUNO, M., AND NUMA, S. Expression of functional sodium channels from cloned cDNA. *Nature Lond.* 322: 826–828, 1986.
35. NUMANN, R. E. AND WONG, R. K. S. Voltage-clamp study of GABA response desensitization in single pyramidal cells dissociated from the hippocampus of adult guinea pigs. *Neurosci. Lett.* 47: 289–294, 1984.
36. OERTEL, W. H., SCHMECHEL, D. E., MUGNAINI, E., TAPPAZ, M. L., AND KOPIN, I. J. Immunocytochemical localization of glutamate decarboxylase in rat cerebellum with a new antiserum. *Neuroscience* 6: 2715–2735, 1981.
37. PATLAK, J. AND ORTIZ, M. Slow currents through single sodium channels of the adult rat heart. *J. Gen. Physiol.* 86: 89–104, 1985.
38. PATLAK, J., ORTIZ, M., AND HORN, R. Opentime heterogeneity during bursting of sodium channels in frog skeletal muscle. *Biophys. J.* 49: 774–777, 1986.
39. PEGRAM, C. N., ENG, L. F., WIKSTRAND, C. J., MCCOMB, R. D., LEE, Y. L., AND BIGNER, D. D. Monoclonal antibodies reactive with epitopes re-

stricted to glial fibrillary acidic proteins of several species. *Neurochem. Pathol.* 3: 119–138, 1985.

40. QUANDT, F. N. Effects of slow inactivation on properties of single Na^+ channels measured in the absence of fast inactivation. *Soc. Neurosci. Abstr.* 13: 674, 1983.
41. STAFSTROM, C. E., SCHWINDT, P. C., CHUBB, M. C., AND CRILL, W. E. Properties of persistent sodium conductance and calcium conductance of layer V neurons from cat sensorimotor cortex in vitro. *J. Neurophysiol.* 53: 153–170, 1985.
42. STAFSTROM, C. E., SCHWINDT, P. C., AND CRILL, W. E. Negative slope conductance due to a persistent subthreshold sodium current in cat neocortical neurons in vitro. *Brain. Res.* 236: 221–226, 1982.
43. STÜHMER, W., METHFESSEL, C., SAKMANN, B., NODA, M., AND NUMA, S. Patch clamp characterization of sodium channels expressed from rat brain cDNA. *Eur. Biophys. J.* 14: 131–138, 1987.
44. THOMPSON, S. M., MASUKAWA, L. M., AND PRINCE, D. A. Temperature dependence of intrinsic membrane properties and synaptic potentials in hippocampal CA1 neurons *in vitro*. *J. Neurosci.* 5: 817–824, 1985.
45. WEISS, R. E. AND HORN, R. Functional differences between two classes of sodium channels in developing rat skeletal muscle. *Science Wash. DC* 233: 361–364, 1986.
46. WOLLNER, D. A. AND CATTERALL, W. A. Localization of sodium channels in axon hillocks and initial segments of retinal ganglion cells. *Proc. Natl. Acad. Sci. USA* 83: 8424–8428, 1986.